Analytical and Semi-Analytical Approaches to the Third-Body Perturbation in Nearly Co-Orbital Regimes

Rita Neves^{a}*, Joan-Pau Sánchez^{a}, Camilla Colombo^{b}, Elisa Maria Alessi^{c}

^{a} *School of Aerospace, Cranfield University, College Road, Cranfield MK43 0AL, United Kingdom*, {r.neves, jp.sanchez}@cranfield.ac.uk
^{b} *Politecnico di Milano, Department of Aerospace Science and Technology, 20156, Milano, Italy*, camilla.colombo@polimi.it
^{c} *Istituto di Fisica Applicata 'Nello Carrara'— Consiglio Nazionale delle Ricerche (IFAC-CNR), Via Madonna del Piano 10, 50019 Sesto Fiorentino (FI), Italy*, em.alessi@ifac.cnr.it
* Corresponding Author

Abstract

This paper studies a range of formulations for third-body motion, based on the disturbing function derived from the Hamiltonian of the Circular Restricted Three-Body Problem (CR3BP). The main one is the well known Keplerian Map (KM), derived from a first-order Picard iteration on the Lagrange Planetary Equations. Three additional strategies to model the third-body effect are generated. The first is the Periapsis-Apoapsis-Periapsis Keplerian Map (PAP-KM), a semi-analytical formulation using the eccentric anomaly as the independent variable. The second is the Euler Keplerian Map (EK Map), a model for long time propagation that uses an Euler method to obtain an accurate evolution of the orbital elements throughout the motion. Finally, the third method is an approximate analytical solution for the evolution of the semi-major axis of the motion, obtained via a Taylor expansion of the eccentricity. These formulations are contrasted with the original KM model and show similar dynamical behaviour, with a decrease in computational time. Furthermore, all of them prove to be more accurate within their application limits.

Keywords:(Third-body effect; Trajectory design; Keplerian Map; Disturbing function)

Nomenclature
μ: Normalised gravitational parameter
$\mathcal{R}$: Disturbing function
$\mathcal{U}_{3B}$: Keplerian Third-Body Potential
$\mathcal{T}$: Taylor series function approximation

Acronyms
Keplerian Map (KM)
Periapsis-Apoapsis-Periapsis Keplerian Map (PAP-KM)
Euler-Keplerian Map (EK Map)
Circular-Restricted Three-Body Problem (CR3BP)
Lagrange Planetary Equations (LPO)
Near-Earth Asteroid (NEA)
Guidance, Navigation & Control (GNC)

1. Introduction

Since the beginning of space exploration, close encounters with celestial bodies in the Solar System have been exploited to change the motion of a spacecraft. Gravity assists are such an example; since they take place inside the planet's sphere of influence, the patched conics approximation is a good model for their computation. This, however, simplifies the spacecraft's motion as to be affected by only one celestial body at a time. Higher accuracy approaches, such as the three-body problem, model a simultaneous attraction of two bodies and its application domain extends beyond the classical sphere of influence.

In between these approaches, perturbation techniques exist to account for the effect of the secondary object in addition to the main attractive body, well outside the former's sphere of influence [1]. In this region, the spacecraft's trajectory can be greatly affected by the secondary body's perturbation, especially in the case of co-orbital regimes of motion, in which the spacecraft moves in a nearly 1:1 resonance with the perturbing body. Using the Sun-Earth system as an example, these kinds of trajectories are extremely useful for near-Earth asteroid (NEA) capture mission designs [2], or long-term disposal strategies for spacecraft [3].

One of these techniques is the Keplerian Map (KM), a well-known method to compute the change of the orbital elements throughout one period of the motion due to the third-body effect in the regime of distant encounters outside the secondary body's sphere of influence. This model can be used in any system of small gravitational parameter, such as the Sun-Earth one. Its development started with the works of Petrosky and Broucke [4] and of Chirikov and Vecheslavov [5]; the concept was then continued by Ross and Scheeres [6] to study distant flybys in the planar CR3BP. Later on, it was expanded by Alessi

and Sánchez [7] for three-dimensional applications.

The aim of this paper is to ultimately study the disturbing function in which the KM is based on, and explore its potentialities for preliminary mission design. Thus, three formulations for the variation of a spacecraft's orbital elements caused by the secondary body's perturbation are described. The first is a full analytical approximation of one of the orbital elements of motion. The second is a semi-analytical method to compute the variation or orbital elements for one period, akin to the original KM. The third employs a numerical integration of the KM equations using an Euler method.

This paper is organised as follows: Section 2 provides a brief overview on common methods to model the third-body effect. Section 3 presents the derivation of the disturbing function of the KM from the Hamiltonian of the CR3BP. Section 4 describes the three main formulations for the application of the disturbing function: numerical, semi-analytical and analytical, and provides the approximations and formulae involved in achieving the latter. Section 5 analyses the original KM and expands it into two new models: the PAP-KM and the EK Map. Finally, Section 6 summarises current findings and highlights areas for future work.

2. **Modelling the Third-Body Effect**

There are several well-known methods to model the motion of an object in a three-body system, given adequate approximations. The ones compared to the methods presented in the paper later on are revised below.

2.1 *The Circular-Restricted Three Body Problem*

When computing trajectories in the Solar System, the complexity of the model of motion increases with the number of bodies interacting. Beyond the two-body problem, the motion of any system with three or more objects has no general analytical solutions. Consequently, the main strategy to compute motion in a three-body system is the CR3BP, whose equations of motion are solved using a numerical integrator. This framework appears as a simplification of the three-body problem, in which the third body's mass is deemed insignificant compared to the other two, the primaries, and their orbits are circular around each other [8].

The CR3BP is typically represented in the synodic reference frame; all the physical quantities are normalised in such a way that both the sum of the primaries' masses and the distance that separates them is equal to 1 [9]. The normalised position $\{x, y, z\}$ and velocity $\{\dot{x}, \dot{y}, \dot{z}\}$ in the CR3BP obey the following equations of motion:

$$\ddot{x} - 2\dot{y} - x = -\frac{(1-\mu)(x+\mu)}{r_1{}^3} - \frac{\mu(x-1+\mu)}{r_2{}^3}$$
$$\ddot{y} + 2\dot{x} - y = -\frac{(1-\mu)y}{r_1{}^3} - \frac{\mu y}{r_2{}^3}$$
$$\ddot{z} = -\frac{(1-\mu)z}{r_1{}^3} - \frac{\mu z}{r_2{}^3} \quad (1)$$

where r_1 and r_2 are the distances to each of the primaries and $\mu = \frac{m_2}{m_1 + m_2}$ is the normalised gravitational parameter of the system.

2.2 *Variation of Parameters*

Variational methods compute the *variation* in the orbital parameters of a third body caused by an additional gravitational force to the central one [10]. In other words, they are ways to account for minor disruptive accelerations in an orbit besides the gravitational effects due to a point mass potential. Depending on the orbit that is being analysed, these can be caused by the non-spherical shape of planets, atmospheric drag, solar radiation pressure or the gravitational attraction of other celestial bodies, the case dealt with in this paper.

Most variational methods have in common that, instead of numerically integrating the orbits directly, only deviations from a two-body solution are considered. In this way, the spacecraft's motion is studied in the two-body problem, but certain regions of movement are considered to be perturbed by additional celestial bodies. This perturbation is described by a disturbing function $\mathcal{R}$, which can be derived using the Hamiltonian of the system.

3. **The Keplerian Third-Body Potential**

The Keplerian Third-Body Potential has been previously used in methods such as the aforementioned KM. Its corresponding disturbing function is used to describe the third-body perturbation in a planetary configuration of small gravitational parameter, such as the Sun-Earth or Jupiter-Callisto systems.

3.1 *Derivation of the Disturbing Function*

In order to derive the Keplerian Third-Body Potential, the Hamiltonian of the three-body problem is formulated in this inertial reference frame:

$$\mathcal{H}_{3B} = \frac{1}{2}(p_x^2 + p_y^2 + p_z^2) - \frac{1-\mu}{r_1} - \frac{\mu}{r_2} \quad (2)$$

in which r_1 and r_2 are the distances from the third body to the primary and secondary, respectively. In order to reach a barycentric notation, r_1 and r_2 have to be written

as functions of the distance to the barycentre r using polar coordinates $\{x = r\cos\theta; \sqrt{y^2 + z^2} = r\sin\theta\}$:

$$r_1^2 = (r\cos\theta + \mu)^2 + (r\sin\theta)^2 \tag{3}$$

$$r_2^2 = (r\cos\theta - 1 + \mu)^2 + (r\sin\theta)^2 \tag{4}$$

where θ is the angle between r and the Sun-Earth line, as it can be seen on Figure 1.

Starting with the development of r_1 into a function of r,

$$r_1^2 = r^2 + \mu^2 + 2r\mu\cos\theta \Leftrightarrow$$

$$\Leftrightarrow \frac{1}{r_1} = \frac{1}{r}\frac{1}{\sqrt{1 + 2\cos\theta\frac{\mu}{r} + (\frac{\mu}{r})^2}} \tag{5}$$

Assuming a Taylor expansion around $\mu = 0$ for the terms with r_1 and r_2:

$$\frac{1-\mu}{r_1} \approx \frac{1}{r} + \mu\left(-\frac{1}{r} - \frac{\cos\theta}{r^2}\right) + \mathcal{O}(\mu^2) \tag{6}$$

$$\frac{\mu}{r_2} \approx \frac{\mu}{\sqrt{r^2 - 2r\cos\theta + 1}} + \mathcal{O}(\mu^2) \tag{7}$$

$$\mathcal{H}_{3B} = \mathcal{K} + \mathcal{U} + \mathcal{O}(\mu^2) \tag{8}$$

in which:

$$\mathcal{K} = \frac{1}{2}(p_x^2 + p_y^2 + p_z^2) - \frac{1}{r} \tag{9}$$

$$\mathcal{U}_{3B} = \mu\left(\frac{1}{r} + \frac{\cos\theta}{r^2} - \frac{1}{\sqrt{1 + r^2 - 2r\cos\theta}}\right) \tag{10}$$

The disturbing function $\mathcal{R}$ is easily computed using the Keplerian Third-Body Potential, as $\mathcal{R} = -\mathcal{U}_{3B}$.

It is important to denote that the movement is not made in the synodic reference frame: it is inertial, Sun-centred, but measured from the Earth axis. This will hence be referred to as an *Earth-pointing reference frame*. This is easily perceived in Figure 1. The inertial reference frame is represented by $\{X, Y, Z\}$, but the spacecraft is observed from the Earth-pointing one. It follows that a new quantity has to be introduced: Ω_{Rot}, which replaces the traditional Ω in the orbital elements. This quantity is the rotational longitude of the ascending node of the spacecraft, defined in such a way that the system's x-axis is aligned with the Earth [7]. In this way, Ω_{Rot} is defined as:

$$\Omega_{Rot} = \Omega - \nu_\oplus \tag{11}$$

Following Alessi and Sánchez [7], $\nu_\oplus$ can be formulated as a function of the third body's orbital elements. To
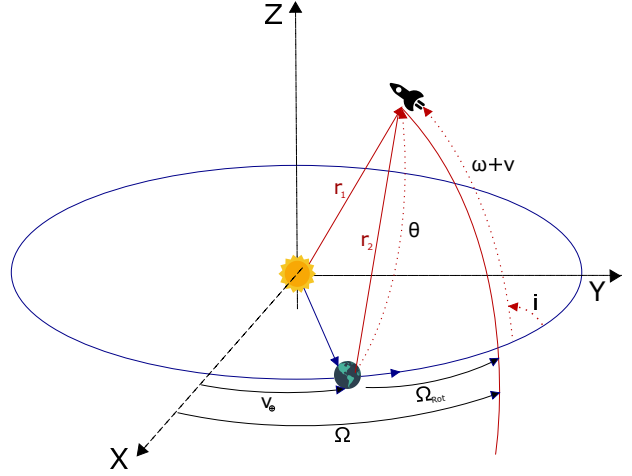

Fig. 1: Three-dimensional geometry of the three-body problem in the inertial reference frame

achieve this, the following laws of planetary motion are expanded:

$$M_\oplus = n_\oplus(t - t_0)$$

$$M_{3B} = n_{3B}(t - t_0) \tag{12}$$

Considering a circular Earth motion (with dimensionless variables, $n_\oplus = 1$) and the equations above, Earth's mean anomaly can be described using purely third body orbital elements in this manner:

$$\frac{M_\oplus}{M_{3B}} = \frac{n_\oplus}{n_{3B}} \tag{13}$$

$$M_\oplus = \frac{M_{3B}}{n_{3B}}$$

$$\nu_\oplus \approx t_\oplus = \frac{M_{3B}}{n_{3B}} - t_0 \equiv \sqrt{\frac{a_{3B}^3}{1 - \mu}}M_{3B}$$

3.2 Formulations of $\mathcal{R}$

The disturbing function derived from the Keplerian Third-Body Potential is highly dependant on two terms: r and $\cos\theta$. Their formulation can be obtained based on either the true anomaly, the method used by Alessi and Sánchez [7], or the eccentric anomaly. These will be here described, and the differences between formulations highlighted.

3.2.1 Formulation in True Anomaly

In this formulation, the quantity r is well known in literature, while $\cos\theta$ is defined using the spherical trigonometric relations determined from Figure 1

$$r = \frac{a(1 - e^2)}{1 + e \cos \nu} \tag{14}$$

$$\cos \theta = \cos \Omega_{Rot} \cos(\omega + \nu) + \sin \Omega_{Rot} \sin(\omega + \nu) \cos i$$

Furthermore, Equation 13 can be further expanded into this:

$$\nu_\oplus \approx \sqrt{\frac{a_{3B}^3}{1 - \mu}} \left[2 \arctan\left(\sqrt{\frac{1 - e}{1 + e}} \tan\left(\frac{\nu_{3B}}{2} \right) \right) \tag{15} \right.$$

$$\left. - \frac{e\sqrt{1 - e^2} \sin \nu_{3B}}{1 + e \cos \nu_{3B}} \right] - t_0$$

From Equation 15, one can easily identify a singularity corresponding to $\nu_{3B} = \pi + 2\pi k, k \in \mathbb{Z}$.

3.2.2 Formulation in Eccentric Anomaly

The formulation of the disturbing function can also be done as a function of the eccentric anomaly E in order to avoid the problem of describing $\nu_\oplus$ as an arctangent of a tangent function, which is not smooth. This is simply made by replacing the values of r and $\cos \theta$ by Equations 16, obtained using well-known formulas [10]:

$$r = a(1 - e \cos E) \tag{16}$$

$$\cos \theta = \cos i \sin \Omega_{Rot} \times$$

$$\frac{(\sqrt{1 - e^2} \cos \omega \sin E(-e + \cos E) \sin \omega)}{-1 + e \cos E} +$$

$$\frac{\cos \Omega_{Rot}((e - \cos E) \cos \omega + \sqrt{1 - e^2} \sin E \sin \omega)}{-1 + e \cos E} \tag{17}$$

Finally, Equation 13 becomes:

$$\nu_\oplus \approx \frac{E - e \sin E}{n} \tag{18}$$

The equations for r and $\nu_\oplus$ become clearly less complex, while the opposite happens for $\cos \theta$. Still, this formulation has the aforementioned advantage of lacking singularities (except when $e = 1$, which is disregarded since the orbit is parabolic).

4. Formulations for the Third-Body Effect

The Keplerian Third-Body Potential can be used in many different ways, depending on the application. In this document, the different possible formulations obtained by exploiting $\mathcal{R}$ are detailed. Their summary is presented in Table 1.

Table 1: Different Formulations using the Disturbing Function $\mathcal{R}$ to compute the evolution of the orbital element set $\mathcal{K}$

Formulation	Mathematical Representation
Numerical	$\frac{d\kappa}{dt} = \left(f\left(\kappa, \frac{d\mathcal{R}}{d\kappa} \right) \right)^*$
Semi-Analytical	$\Delta\kappa = \int_{t_i}^{t_f} f\left(\kappa, \frac{d\mathcal{R}}{d\kappa} \right) dt$
Analytical	$\Delta\kappa = \mathcal{T}(\kappa, t_f) - \mathcal{T}(\kappa, t_i)$

* Computed with a numerical propagator

4.1 Numerical: Lagrange Planetary Equations

After obtaining the disturbing function $\mathcal{R}$ from the Keplerian Third-Body Potential, the Lagrange Planetary equations (LPE) can be used to obtain the equations of motion of the perturbed body [10]:

$$\frac{da}{dt} = \frac{2}{na} \frac{\partial \mathcal{R}}{\partial M}$$

$$\frac{de}{dt} = \frac{1 - e^2}{n\, a^2 e} \frac{\partial \mathcal{R}}{\partial M_0} - \frac{\sqrt{1 - e^2}}{n\, a^2 e} \frac{\partial \mathcal{R}}{\partial \omega}$$

$$\frac{di}{dt} = -\frac{1}{na^2\sqrt{1 - e^2} \sin i} \frac{\partial \mathcal{R}}{\partial \Omega} - \frac{\cos i}{na^2\sqrt{1 - e^2} \sin i} \frac{\partial \mathcal{R}}{\partial \omega}$$

$$\frac{d\Omega}{dt} = \frac{1}{n\, a^2 \sqrt{1 - e^2} \sin i} \frac{\partial \mathcal{R}}{\partial i}$$

$$\frac{d\omega}{dt} = \frac{\sqrt{1 - e^2}}{n\, a^2 e} \frac{\partial \mathcal{R}}{\partial e} - \frac{\cos i}{na^2\sqrt{1 - e^2} \sin i} \frac{\partial \mathcal{R}}{\partial i}$$

$$\frac{dM_0}{dt} = n - \frac{2}{n\, a} \frac{\partial \mathcal{R}}{\partial a} + \frac{1 - e^2}{na^2 e} \frac{\partial \mathcal{R}}{\partial e} \tag{19}$$

The derivatives of the disturbing function take the form of Equation 20, in which $\mathcal{K}$ is one of the regular orbital elements. The derivatives of r and $\cos \theta$ with respect to each element are trivial to compute, given their formulation in Equation 14 or 16, depending on the independent variable.

$$\frac{\partial \mathcal{R}}{\partial \mathcal{K}} = -\frac{1}{r^2} \frac{\partial r}{\partial \mathcal{K}} + \frac{1}{r^2} \frac{\partial \cos \theta}{\partial \mathcal{K}} - \frac{2 \cos \theta}{r^3} \frac{\partial r}{\partial \mathcal{K}} + \tag{20}$$

$$\frac{1}{(r^2 - 2r \cos \theta + 1)^{\frac{3}{2}}} \left(r \frac{\partial r}{\partial \mathcal{K}} - \cos \theta \frac{\partial r}{\partial \mathcal{K}} + r \frac{\partial \cos \theta}{\partial \mathcal{K}} \right)$$

4.2 Semi-Analytical: The Keplerian Map

The KM is a well-known model to measure an orbital element change throughout one period of motion caused by the third-body perturbation. It is computed as a semi-analytical method [7], as it employs a first Picard iteration on Equations 19. Ultimately, this yields the changes in orbital elements after a full orbit of the third-body.

$$\Delta a = \frac{2}{na} \int_{t_i}^{t_f} \frac{\partial \mathcal{R}}{\partial M_0} dt$$

$$\Delta e = \frac{(1-e^2)}{na^2 e} \int_{t_i}^{t_f} \frac{\partial \mathcal{R}}{\partial M_0} dt - \frac{\sqrt{1-e^2}}{na^2 e} \int_{t_i}^{t_f} \frac{\partial \mathcal{R}}{\partial \omega} dt$$

$$\Delta i = -\frac{1}{na^2\sqrt{1-e^2}\sin i} \int_{t_i}^{t_f} \frac{\partial \mathcal{R}}{\partial \Omega} dt +$$

$$\frac{\cos i}{na^2\sqrt{1-e^2}\sin i} \int_{t_i}^{t_f} \frac{\partial \mathcal{R}}{\partial \omega} dt$$

$$\Delta\Omega = \frac{1}{n\sqrt{1-e^2}a^2 \sin i} \int_{t_i}^{t_f} \frac{\partial \mathcal{R}}{\partial i} dt$$

$$\Delta\omega = \frac{\sqrt{1-e^2}}{na^2 e} \int_{t_i}^{t_f} \frac{\partial \mathcal{R}}{\partial e} dt -$$

$$\frac{\cos i}{na^2\sqrt{1-e^2}\sin i} \int_{t_i}^{t_f} \frac{\partial \mathcal{R}}{\partial i} dt$$

$$\Delta M_0 = -\frac{2}{na} \int_{t_i}^{t_f} \frac{\partial \mathcal{R}}{\partial a} dt - \frac{1-e^2}{na^2 e} \int_{t_i}^{t_f} \frac{\partial \mathcal{R}}{\partial e} dt \quad (21)$$

As the equations are integrated over a given period, this formulation proves to be much faster than the straightforward numerical propagation of the LPE in Equation 19. However, given that the semi-major axis is changing throughout the motion, the orbital period is accordingly altered, making the time an unsuitable integration limit. Following that the orbital element update is computed for one full orbit, it is then more convenient to perform the integration by taking either the true or eccentric anomaly as independent variable, depending on the chosen formulation.

In order to correctly modify Equations 21 for this purpose, some relations need to be stated. For both the cases of the true and eccentric anomalies, the corresponding formulae are obtained from Chao [11]:

$$\frac{dt}{d\nu} = \frac{r^2}{na^2\sqrt{1-e^2}}, \frac{dt}{dE} = \frac{1-e\cos E}{n} \quad (22)$$

$$\frac{\partial \mathcal{R}}{\partial M_0} = \frac{a^2\sqrt{1-e^2}}{r^2} \frac{\partial \mathcal{R}}{\partial \nu}, \frac{\partial \mathcal{R}}{\partial M_0} dt = \frac{1}{n} \frac{\partial \mathcal{R}}{\partial E} dE \quad (23)$$

Thus, as previously discussed, Equations 15 and 18 allow the computation of Ω_{Rot} as a function of the true or eccentric anomaly of the third-body, which in turn is the independent integration variable, transformed from the normalised time. This makes the reference frame for the KM, previously defined as the Earth-pointing reference frame, time-dependent; thus, Equations 15 and 18 are the mapping from the normalised time to the independent variable.

The original KM, which will be mentioned throughout this paper, makes the orbital elements update at each periapsis passage, with integration over the true anomaly ($\nu_i = -\pi, \nu_f = \pi$) [7]. These changes are then added to the previously known orbital elements to obtain the updated motion.

In this way, another physical quantity can be introduced: the parameter α_P, representing the phasing of the third body with the disturbing one, while the first is at periapsis (hence the subscript). In other words, it is the angle between the Sun-Earth axis and the projection to the ecliptic plane of the line connecting Sun to third body, using the synodic reference frame. After one full period, the new phasing can be computed with an update in α_P, using Equation 24.

$$\Delta\alpha_P : 2\pi - 2\pi\sqrt{\frac{a^3}{1-\mu}} \quad (24)$$

Given that α_P is a function of the longitude of the ascending node, Equation 24 can simply be used instead of the update $\Delta\Omega$ in Equations 21 [7]. Finally, gathering Equations 21 and 24, the action of the KM can be represented by the mapping $\mathcal{M}$:

$$\mathcal{M} : \{a, e, i, \omega, M_0 | \alpha_{P_n}\}$$
$$\mapsto \{\Delta a, \Delta e, \Delta i, \Delta\omega \Delta M_0 | \alpha_{P_{n+1}}\} \quad (25)$$

These equations do not need to be computed throughout the entire motion; instead, they are used inside a neighbouring region of the Earth, within which its gravitational perturbation is non-negligible. This region is defined by an interval of α values, shown to capture the extent of the disturbing effect; outside it, the gravitational perturbation of the Earth is so small that can be effectively neglected. Alessi and Sánchez [7] have determined this region to be $\alpha \leqslant |\pi/8|$.

4.3 Analytical: Taylor Approximation

A full analytical formulation of Equations 19 is impossible to concoct. There are two immediate factors behind this, and both have to do with the independent variable (true or eccentric anomaly).

- **The mapping from time to the independent variable**, using Equations 15 and 18: it cannot be derived with the remaining expression in Equation 20, having to stay unchanged. Still, it adds a considerable amount of complexity to the equations.

- **The term introduced by Equation 23**: depending on the independent variable, it adds another layer of complexity to the integration.
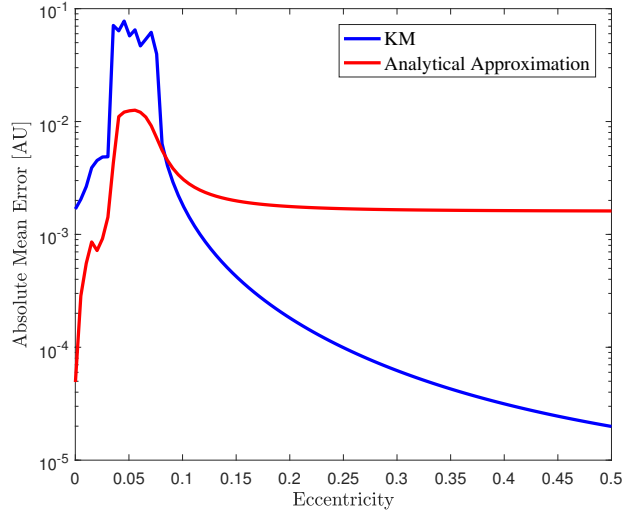
Fig. 2: Absolute mean error in semi-major axis update after one period as a function of the eccentricity. Error in logarithmic scale, averaged for 10,000 initial orbital conditions

Fig. 3: Semi-major axis evolution of one orbital period for elements $\{a = 1.03, e = 0.001, i = 0.001, \Omega = 5.93, \omega = 2.32, E = 0\}$

Still, approximations can be employed to obtain an analytical solution to some of the differential equations. The process can be broken down in the following manner: a Taylor series is used to approximate Equation 20 for each orbital element. Then, this expression is inserted back into Equations 19, which may be solved analytically.

For this paper, a Taylor series of order zero of the eccentricity was successfully employed (other orbital elements and orders of approximation were tried, without any success). The resulting analytical description of the semi-major axis can be found in Equation 26. However, the two factors listed above make it so that the semi-major axis is the only element in which the equations are simple enough to obtain an analytical formulation, without resorting to any other approximation.

Equation 26 is the analytical solution found for the evolution of the semi-major axis. It provides a simple expression to quickly compute the behaviour of the orbital element; nevertheless, it is limited by the fact that the orbit must have a very low eccentricity. In order to understand what kind of error would be obtained as a function of the latter parameter, 10,000 initial conditions are computed. The plot obtained in Figure 2 represents the average absolute error (as compared to the CR3BP) for each eccentricity value, for both Equation 26 and the original KM.

As it can be seen, the analytical approximation actually works better than the KM up until an eccentricity of roughly 0.1. This is explained by the fact that the analytical simplification avoids the well-known singularity in eccentricity of the LPE. This is extremely useful when computing the behaviour of low eccentricity orbits, like the ones of many NEA.
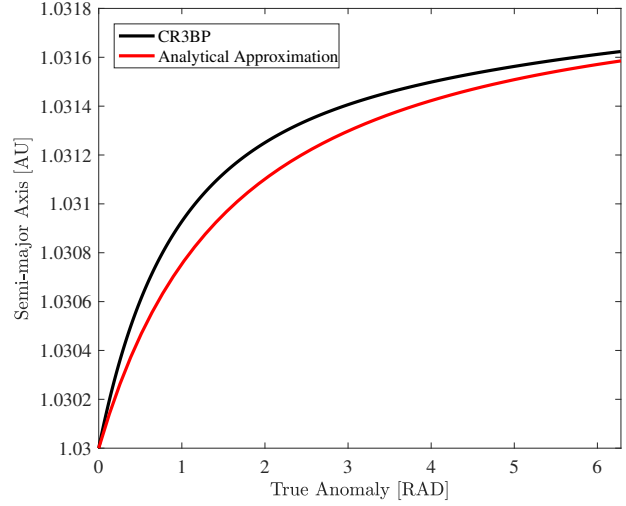
$$
\begin{aligned}
a \approx \frac{2\mu}{na} \Bigg(& \frac{1}{(n-1)\sqrt{1 + a^2 - 2a\cos(E - \frac{E}{n} + \omega + \Omega)}} \\
& - \frac{1}{4a^2(n^2 - 1)} \bigg(2(n-1)\cos\left(E + \frac{E}{n} + \omega - \Omega\right) \\
& + (1-n)\cos\left(E + \frac{E}{n} - i + \omega - \Omega\right) \\
& + (1-n)\cos\left(E + \frac{E}{n} + i + \omega - \Omega\right) \\
& + 2(1+n)\cos\left(E - \frac{E}{n} + \omega + \Omega\right) \\
& + (1+n)\cos\left(E - \frac{E}{n} - i + \omega + \Omega\right) \\
& + (1+n)\cos\left(E - \frac{E}{n} + i + \omega + \Omega\right) \bigg) \Bigg) + \mathcal{O}(e^1)
\end{aligned}
$$
(26)

In order to better visualise the behaviour of Equation 26, Figure 3 analyses one of the initial conditions for $e = 0.001$. It shows the one-period propagation of the semi-major axis for both the CR3BP and the analytical approximation. It can be seen that, while the final result is slightly different, the evolution of the orbital elements is very similar.
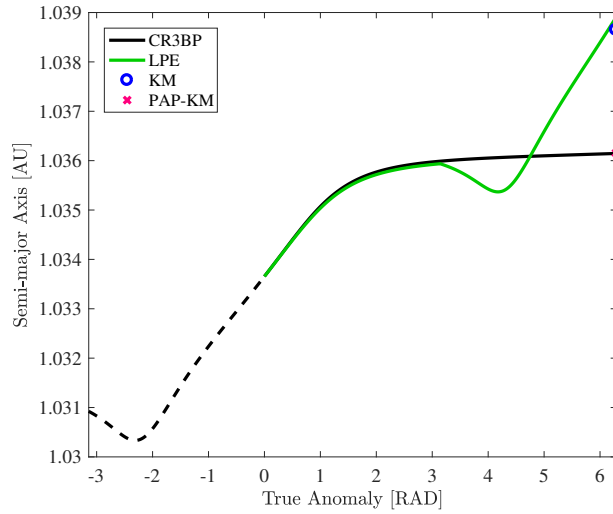
Fig. 4: Semi-major axis evolution of one orbital period for asteroid 2018 AV2. Extra back-propagation of half a period for the CR3BP in a dashed line

5. Expansions

Given the analysis of the characteristics and limitations of the KM conducted on Section 4, some improvements can effectively be obtained. This section will explore some of these ideas and examine any achievable enhancements in accuracy.

5.1 The PAP-KM

As detailed in Sub-section 4.2, the original KM was obtained using the true anomaly as the independent variable for the integration. The interval $\left[-\pi, \pi\right]$ was chosen in order to avoid numerical errors, and it also bypasses the non-smoothness of the mapping on Equation 15. As such, the new conditions at periapsis are taken from the changes between apoapses.

However, this approximation will naturally yield accuracy errors, especially in cases where the orbital elements are noticeably altered. Figure 4 highlights one example: it shows the propagation of asteroid 2018 AV2 in its closest pass near the Earth, in 2037. The values highlighted are the orbital propagation in different frameworks: the CR3BP, the propagation of the LPE in Equations 19 with the true anomaly as the independent variable, and the original KM. The dashed line corresponds to the CR3BP propagation in the section from $-\pi$ to 0. It can be seen that the Δa given by the KM is actually similar to the $-\pi$ to π evolution given by the CR3BP. However, this Δa does not match the period from 0 to 2π, causing a large error when updating the new semi-major axis.
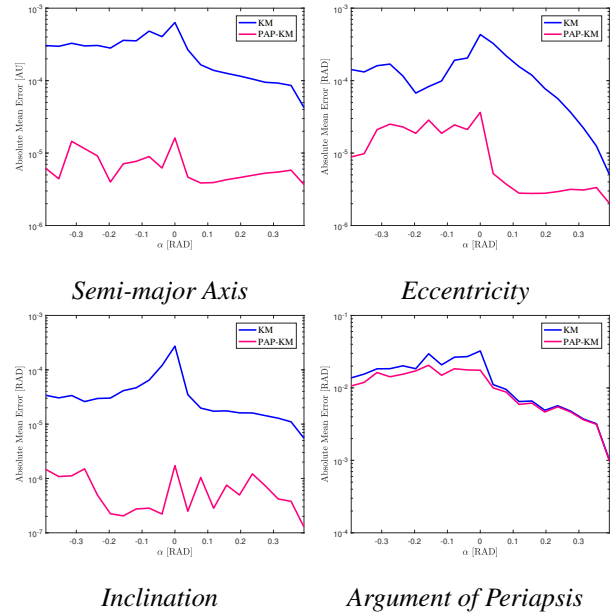
The alternative is to use the Periapsis-Apoapsis-

Fig. 5: Absolute mean error after one period as a function of initial α_P. Error in logarithmic scale, averaged for 10,000 initial orbital conditions

Periapsis-Keplerian Map (PAP-KM). This is simply done by implementing the KM using the eccentric anomaly and changing the propagation interval to $\left[0, 2\pi\right]$, as detailed in Sub-section 3.2.2. The result can also be found in Figure 4, depicting the actual expected value for the semi-major axis update.

For comparison on the performance of the KM and the PAP-KM after one period of motion, these two methods were compared with the CR3BP for 10,000 different initial conditions. The averaged result for each starting α_P was plotted in Figures 5. As it can be observed, the PAP-KM case shows a much smaller error after just one period, which confirms it as a better alternative to the original KM.

5.2 The EK Map

An obvious drawback of the KM is that, as opposed to the numerical method, the parameter update is made using only its initial value, regardless of its evolution throughout the orbit. In order to account for this effect, the PAP-KM can be interpolated with an Euler method. This will yield an approximation of the instantaneous element change and also avoid possible integration errors from the PAP-KM. This method is hence referred to as the Euler-Keplerian Map (EK Map).

The number of computation intervals was chosen for the computational time taken by the KM and the EK-Map to be the same, which yielded 21 points. The algorithm's
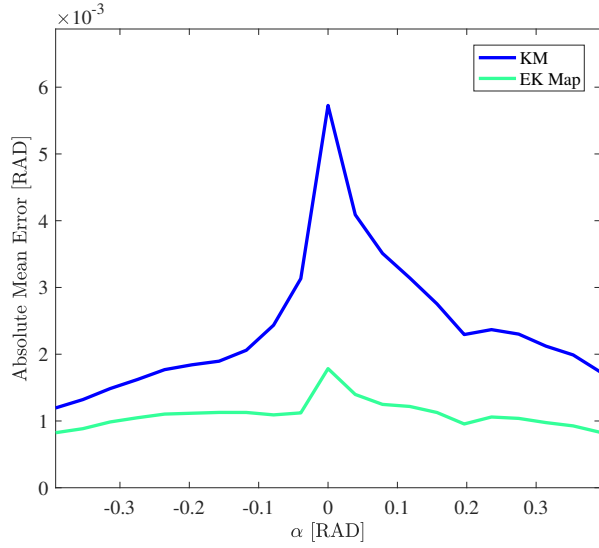
Fig. 6: Absolute mean error after one period as a function of initial α_P. Error averaged for 10,000 initial orbital conditions

Semi-major Axis   *Eccentricity*

Inclination   *Argument of Periapsis*

Fig. 7: Average absolute error for orbital element update for 21 periods

pseudo-code works in the following manner:

Initialization: $\mathcal{K} = \mathcal{K}_0$; $E = 0$;
while $E < E_{final}$ **do**
    slope = Equation 19;
    $\mathcal{K} = \mathcal{K} + slope*step$;
    $E = E + step$;
end
Algorithm 1: Euler method for computing the evolution of the orbital element $\mathcal{K}$

5.2.1 Phasing Update

As previously discussed, Equation 24 shows that the update is done using only the period of the motion: more concretely, only the semi-major axis is needed. Since this element may be changing steeply throughout the orbit, the contribution of an instantaneous semi-major axis would be a great advantage. This can be accurately done using the Euler method on the semi-major axis, as it is done in the EK Map, using Algorithm 1.

In order to verify this claim, the regularly computed α_P in Equation 24 and the one obtained with the semi-major axis instantaneous evolution were compared with the CR3BP for 10,000 different initial conditions, in the same fashion as Figures 5. The absolute error is again shown in Figure 6 as the average of each initial α_P. It can be seen that the instantaneous α update performs much better. This is more obvious in the region closer to the Earth ($\alpha_P \approx 0$), where the semi-major axis is predicted
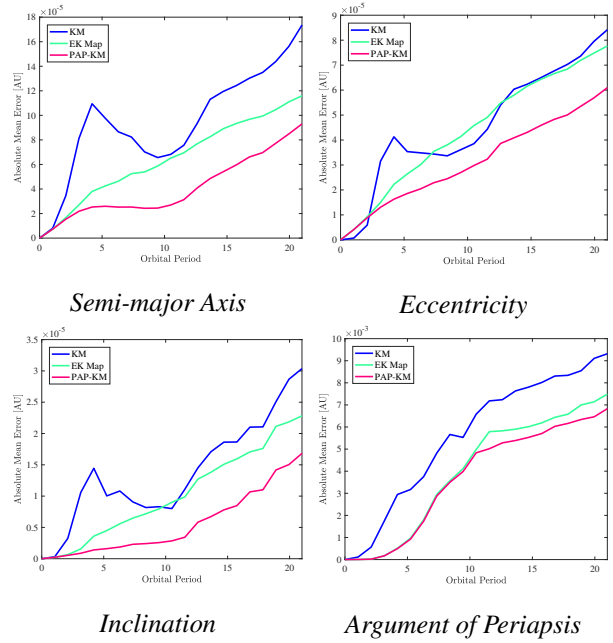
to change more drastically.

It is important to denote that the improvement in the α update can also be done in the PAP-KM, just by adding an extra computation of the instantaneous semi-major axis.

5.3 Long-Term Propagation

A short analysis of the long term propagation error for the KM, the PAP-KM (with the instantaneous α provided by Sub-section 5.2.1) and the EK Map is made on Figure 7: 10,000 initial conditions are propagated with the three methods, over 21 periods of motion. At each periapsis, the absolute error of each of this initial conditions is averaged for each model, using the CR3BP propagation as the baseline.

As expected, the error accumulates with the number of periods for all of the orbital elements. For both methods presented in this section, this happens at a much shorter rate than the original KM. While the expectation would be for the EK Map to perform the best, the error provided by the PAP-KM with the instantaneous α is clearly the smallest. This may indicate some problem with the Euler method, or it may be so that small errors when computing the instantaneous orbital elements accumulate faster in this setting.

Finally, similarly to what Ross and Scheeres did for the KM [6], the dynamical behaviour of the EK Map is compared to the CR3BP in Figure 8 in the Jupiter-Callisto system. These show the evolution of the semi-major axis
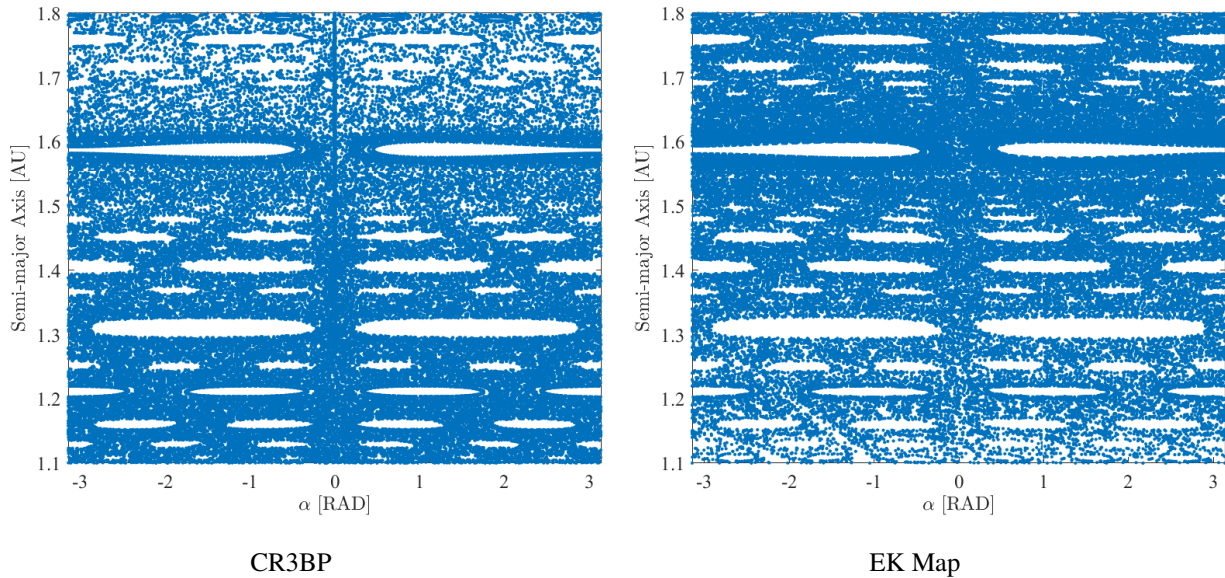
Fig. 8: Plot of the stable resonances in the Jupiter-Callisto system

in a long term propagation, as a function of the initial α_P: each point corresponds to the new semi-major axis after one orbit, computed for roughly 300 periods. The initial conditions were chosen for a $\in$ $\big[1.1,\ 1.8\big]$, avoiding the islands corresponding to stable mean motion resonances of the particle's orbit with Callisto's: these are the white ovals depicted in the plots. It is possible to see that the behaviour of the resonances and islands is maintained, which ultimately confirms the validity of the EK Map.

5.4 Computational Time

Considering the low-fidelity of the methods developed so far, it was considered important to have a decreased computational cost in contrast to the CR3BP. Without any further code optimisations for time, the original KM and the PAP-KM were determined to be respectively 13% and 22% faster than the latter for one period, with the EK Map having the same computational cost as the KM, as explained in Sub-section 5.2. Still, over a full trajectory, the methods described in this paper possess the advantage of being used only in a restricted region of space, as detailed in Sub-section 4.2. For the remaining motion, the model used is the two-body problem, which decreases the overall computational cost immensely.

6. Conclusions

This paper presented a study on approaches to compute the third-body effect based on the Keplerian Third-Body Potential, used to compute the disturbing function of the

Keplerian Map. As it is formulated, the KM is an accurate, low-cost descriptor of the secondary perturbation for third-body motion, provided that the system has a very small gravitational constant μ.

Using the Keplerian Third-Body Potential as the starting point, several different formulations for the third-body effect were devised, their utility depending on the application scenario. From these, three are highlighted: the analytical approximation for the semi-major axis evolution, the PAP-KM and the EK Map. The first can be used for a quick understanding of the behaviour of the orbital element in small eccentricity orbits. The PAP and EK Maps are improvements on the original KM, removing its singularity and taking into consideration steep changes of the orbital elements throughout the period of motion.

A very important characteristic of the formulations is that they can be hybridized and combined together, depending on the application scenario. For example, the analytical prediction of the semi-major axis evolution can be combined with the EK Map method for the evolution of the remaining orbital elements of motion, which can then be transformed into a predictor of the position and velocity of a spacecraft. This is potentially useful for fast online computations and application in GNC algorithms.

Some aspects of these methodologies are very unique and deserve further attention. The time-dependent nature of the reference frame used and how it affects the differential equations is something that needs further consideration. Furthermore, the validity and range of approximations to complement the semi-major axis analytical ex-

pression will be studied in more detail. Finally, future work will also consider the application of these methods in a preliminary trajectory design scenario, such as asteroid capture missions or end-of-life disposal strategies.

Acknowledgements

References

[1] D.A. Vallado. *Fundamentals of Astrodynamics and Applications*, volume 12. Springer Science & Business Media, 2001.

[2] J. P. Sánchez, R Neves, and H Urrutxua. Trajectory Design for Asteroid Retrieval Missions: A Short Review. *Frontiers in Applied Mathematics and Statistics [in publication]*, 2018.

[3] Z. Olikara, Gómez G., and Masdemont J. End-of-life Disposal of Libration Point Orbit Spacecraft. In *64rd International Astronautical Congress*, pages 1–13, 2013.

[4] T.Y. Petrosky and R. Broucke. Area-preserving Mappings and Deterministic Chaos for Nearly Parabolic Motions. *Celestial mechanics*, 42(1-4):53–79, 1987.

[5] R.V. Chirikov and V.V. Vecheslavov. Chaotic Dynamics of Comet Halley. *Astronomy and Astrophysics*, 221:146–154, 1989.

[6] S. D. Ross and D. J. Scheeres. Multiple Gravity Assists, Capture, and Escape in the Restricted Three-Body Problem. *SIAM Journal on Applied Dynamical Systems*, 6(3):576–596, 2007.

[7] E. M. Alessi and J. P. Sánchez. Semi-Analytical Approach for Distant Encounters in the Spatial Circular Restricted Three-Body Problem. *Journal of Guidance, Control, and Dynamics*, 39(2):351–359, 2015.

[8] W. Koon, M. Lo, J. Marsden, and S. D. Ross. Dynamical Systems, the Three-Body Problem and Space Mission Design. *Free online Copy: Marsden Books*, 2008.

[9] V. Szebehely and E. Grebenikov. Theory of Orbits - The Restricted Problem of Three Bodies. *Soviet Astronomy*, 13:364, 1969.

[10] Richard H Battin. *An Introduction to the Mathematics and Methods of Astrodynamics*. American Institute of Aeronautics and Astronautics, 1999.

[11] C. C. Chao. *Applied Orbit Perturbation and Maintenance*. American Institute of Aeronautics, 2005.